Fatigue and fracture toughness properties of large-bloom mixed-microstructure heat-treated steels

D. Firrao[1], P. Matteis[1], P. Russo Spena[1], G.M.M. Mortarino[1],
G. Silva[2], B. Rivolta[2], R. Gerosa[2], M.R. Pinasco[3], M.G. Ienco[3], M. Fabbreschi[3]
[1]DISMIC, Politecnico di Torino, Torino, Italy; [2]Dip. Meccanica, Politecnico di Milano, Milano, Italy; [3]DCCI, Università di Genova, Genova, Italy

Abstract

The standard ISO 1.2738 medium-carbon low-alloy steel have long been used to fabricate plastic molds for large automotive components (bumpers and dashboards) by machining large previously quenched and tempered steel blooms. Due to the bloom size, the heat treatment yields mechanical properties and mixed microstructures continuously varying from surface to core. Alternative steel grades, including both non-standard microalloyed steels, designed for the same production cycle, and precipitation hardening steels, were recently proposed. Results of a large experimental effort concerning the fracture toughness and fatigue properties (as well as other mechanical properties) of plastic mold steel blooms are presented and commented, also on the basis of microstructural and fractographic analysis. These steels generally exhibit low fracture toughness values; in the traditional quench and temper production cycle this characteristic arises from the presence of mixed microstructures, whereas in the precipitation hardened steel the brittleness probably stems from the carbide precipitation strengthening mechanism.

1. Introduction

Large steel molds are employed to form automotive components, such as bumpers and dashboards, by the use of thermoplastic polymers, often glass reinforced. During service a plastic mold is subjected to mechanical and thermal fatigue (up to a few millions cycles) and to wear from reinforced resin flows; stresses can be enhanced by abnormal shop operations.

The molds are commonly machined from large quenched and tempered steel blooms, usually with 1x1 m cross-section and more than 1 m length. Due to the large section, after the heat treatment the bloom microstructures and mechanical properties may vary continuously from surface to core. The successive mold machining may be so deep that microstructures occurring at any depth in the bloom can be found at the mold face. Weld bed deposition operations are often used to modify the mold shape to extend the service life after car body restyling.

The ISO 1.2738 (or 40CrMnNiMo8-6-4 [1]) alloy steel is the most used standard

grade, but it yields inhomogeneous bloom microstructures with low toughness, and it is difficult to weld. Several alternative proprietary steels are employed, with the aim either of yielding more uniform microstructures and better properties throughout the mold sections, or of improving the weldability (often by using a C content lower than 0.3%). These steels include not only quenched and tempered grades, but also precipitation hardenable ones. The precipitation hardening can be done after machining, since it causes only small deformations, and may yield homogeneous results in large molds with complex shapes.
Several commercial blooms were examined in a large research program. A, B and C blooms were quenched and tempered 1.2738 steel blooms produced by different steelmakers. Bloom D consists of a precipitation hardening steel, whereas bloom E consists of a microalloyed quenched-and-tempered one. Although most tests were performed in the condition directly due to the bloom heat-treatment, some specimens were re-heat-treated in small furnaces and tested for comparison; age-hardening tests were also done in laboratory furnaces.
Whereas most results were reported in previous papers [2-7], each addressing in greater detail a subset of the examined steels properties, the present work aims to thoroughly review the main finding and to compare the different steels.

2. Steelwork and Experimental Procedures

The usual bloom production cycle consists of ingot casting, hot forging, and heat treating. Since the bloom and ingot sections are similar, ingot inhomogeneities are reduced by repeated hot-forging elongation and compression cycles. The bloom heat treatment consists of dehydrogenizing, austenitizing, quenching and double tempering. A low tempering temperature is used for age-hardenable steels.
The chemical compositions of the examined blooms were measured by optical emission spectrometry, Tab. 1. The blooms' recorded or estimated forged size and final steelwork heat-treatment temperatures are shown in Tab. 2; D bloom was previously subjected to a preliminary hypercritical heat treatment [5,7]. The L direction defines the long ingot casting and forging axis, whereas the S and T directions are thought to be not differently influenced by the production process. B, C and E blooms were cut to a U shape for fabricating bumper molds, and the residual was used to fabricate series of samples ranging from the surface to the core of the bloom, in direction T. Test results are reported against the distance from one SL forged surface (*depth*) or from the SL mid-plane (*distance from the core*), even if distances from LT or LS surfaces are not exactly equal. D steel samples were obtained within 170 mm depth only.
Re-Heat-Treated (RHT) test samples were made with 1.2738 steel coming from C bloom, as well as with D steel. 1.2738 steel was re-austenitized in the 850 to 870 °C range, and then either fully quenched and tempered up to 590 °C (in 1 or 2 stages), or isothermally treated at 340 or 600 °C. D steel was re-austenitized at 1050 °C, air cooled, and double tempered at 400 °C. Both as-received and RHT D steel samples were age-hardened at 470, 510 or 550 °C for up to 8 h.

Tab. 1. ISO 1.2738 compositional limits and blooms composition, wt.%.

	C	Mn	Cr	Ni	Mo	Si	Nb	V	B	Zr	S	P
ISO 1.2738	0.35 0.45	1.3 1.6	1.8 2.1	0.9 1.2	0.15 0.25	0.2 0.4	n.r.	n.r.	n.r.	n.r.	0 0.03	0 0.03
A	0.46	1.7	2.0	1.1	0.25	0.24	n.d.	0.007	0.0013	n.m.	<0.001	0.010
B	0.39	1.5	2.1	1.0	0.20	0.22	n.d.	0.02	n.d.	n.m.	0.009	0.011
C	0.42	1.5	2.0	1.1	0.21	0.37	n.d.	0.08	n.d.	n.m.	0.002	0.006
D	0.16	0.7	0.2	3.2	3.2	0.22	n.d.	0.08	n.d.	n.m.	0.002	0.005
E	0.28	1.6	1.4	1.1	0.60	0.28	0.02	0.12	0.0013	0.03†	<0.001	0.007

†Estimated n.r.: not restricted n.m.: not measured n.d.: not detected

Tab. 2. Forged size and final steelwork bloom quench and temper heat-treatments.

Bloom	Bloom size (mm)			Austenitizing		Cooling	Tempering temp. (°C)	
	L	T	S	temp. (°C)	grain (µm)	medium	1st	2nd
A	2420*	1140*	1000*	860*	115	air*	600*	
B	2240*	900*	900*	860*	10 - 100†	air*	600*	
C	2970	1285	1190	850	10	oil	590	550
D	2400	1500	500	1020	130	air	400	400
E	2900	1020	1260	950	265	water	590	550

*Estimated from delivered size, test results and/or common usage †Inhomogeneous

Microstructures were examined by both optical and scanning electron microscopy, after mechanical polishing and chemical etching, mostly by Nital. In most cases, the austenitic grain size was measured with the three-circle intercept-count method after special etching (e.g. Bechet-Beaujard).

An electrochemical extraction procedure was used to investigate the precipitates occurring during age hardening. The sample was dissolved in ethanol and hydrochloric acid (10% vol.) and the undissolved second phases were collected on a filter (0.1 mm mesh size). The filter was examined by. X-Ray Diffraction (XRD), by comparison with an unused filter. Moreover, the compacted second phase powder was examined by Energy Dispersion Spectroscopy (EDS).

Mechanical tests were performed at room temperature, according to the relevant ISO and ASTM standards [8,9], unless otherwise specified.

Fracture toughness (K_{Ic}) tests were performed on 35 or 38 mm thick Single Edge Notched Beam (SENB) samples with LT orientation. The P_Q load was often a pop-in maximum, and in some cases, especially in bloom D, the ensuing P_{MAX}/P_Q ratio was larger than 1.1.

Rotating bending fatigue stress-life (S-N) tests were performed according to the staircase method, on smooth 6 mm diam. cylindrical samples, to determine the stress corresponding to a 50% survival probability after $4.2 \cdot 10^6$ cycles.

Fatigue Crack Growth (FCG) tests were performed on 6 mm thick Compact Tension (CT) samples or 12.5 mm thick SENB samples, with LT orientation, constant amplitude sinusoidal loading, and load ratio R = 0.1. The crack length of CT samples was measured optically on both polished sample surfaces; the fatigue

test was interrupted to perform each measurement; crack-length differences between the two sides in excess of 25% of the thickness occurred at times in the low ΔK range (ΔK being the cyclic amplitude of the stress intensity factor). The crack length of SENB samples was monitored continuously, by using a compliance method, and recorded at fixed crack length intervals. The secant method and the incremental polynomial method (of order 2) were used to analyze the ΔK-decreasing and ΔK-increasing datasets, respectively.

3. Microstructures, Hardness and Strength

The Prior Austenitic Grains (PAG) size resulting from the industrial heat-treatment of the three examined 1.2738 steel blooms ranges from 10 to 100 µm (Tab. 2), probably because of their different V content, since V carbides can pin the grain boundaries at the austenitizing temperature used for this steel. The PAG size of D and E blooms is generally larger (Tab. 2), even if they have larger V contents, likely because VC dissolves at the higher austenitization temperatures used for the industrial heat-treatment of these steels. In fact, the steel E PAG size was ~20 µm only after austenitizing tests performed at 885 °C, which is just lower than the estimated VC dissolution temperature for this steel.

The actual microstructure of 1.2738 steel blooms consists mainly of tempered martensite close to the surface, of temper-modified bainite in most of the bloom volume, and of pearlite at core, with a gradual transition among these constituents, determined by the decreasing cooling rate, from surface to core, during the quench stage (Fig. 1). However, in A and B blooms pearlite first appears at a smaller depth and with a less homogeneous distribution (i.e., mainly at PAG boundaries) than in bloom C; moreover, bloom C microstructures are finer due to finer PAGs.

Consistently with the microstructures, the C bloom hardness monotonically decreases from 360 - 380 HV_{100} at surface to 280 HV_{100} at core. On the contrary, in the B bloom the hardness first increases from ~320 HV_{100} at surface to ~350 HV_{100} at mid-depth, and then decreases to ~270 HV_{100} at core; this is probably due to an inhomogeneous (i.e. short) tempering. The yield strength (YS) and ultimate tensile strength (UTS) follow a similar pattern (Fig. 2); due to three-dimensional effects, the C bloom minimum YS and UTS are probably lower than the Fig. 2 minima, which do not correspond spatially with the hardness minimum.

The re-heat-treated 1.2738 steel samples consisted of: pearlite after the 600 °C isothermal treatment; bainite with some untempered martensite after the 340 °C isothermal treatment; tempered martensite after the quench and temper treatments (hardness ~385 HV_{100}, YS ~1050 MPa, UTS ~1180 MPa in most cases).

The E bloom microstructure is overall more homogeneous than the 1.2738 steel blooms, since it consists of tempered martensite and temper-modified bainite in the surface region (Fig. 1c), and of temper-modified bainite only in the mid-depth and core (Fig. 1d) regions; the hardness, YS and UTS are almost constant in the bloom section and close to 375 HV_{100}, 990 and 1145 MPa, respectively (Fig. 2).

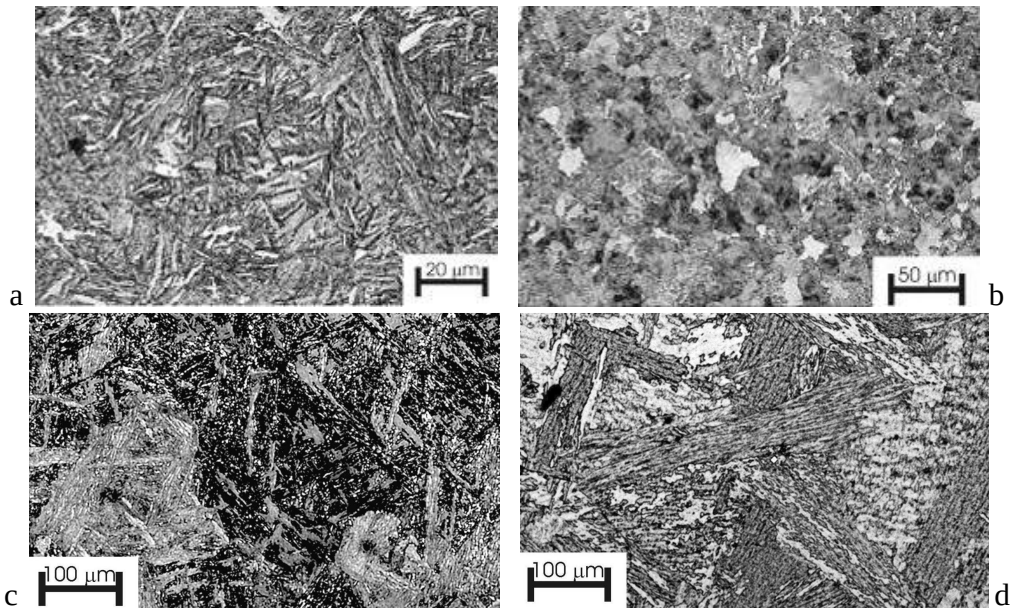

Fig. 1 – Microstructures of blooms C (steel 1.2738) (a,b) and E (c,d) at surface (a,c) and at core (b,d). Optical microscopy.

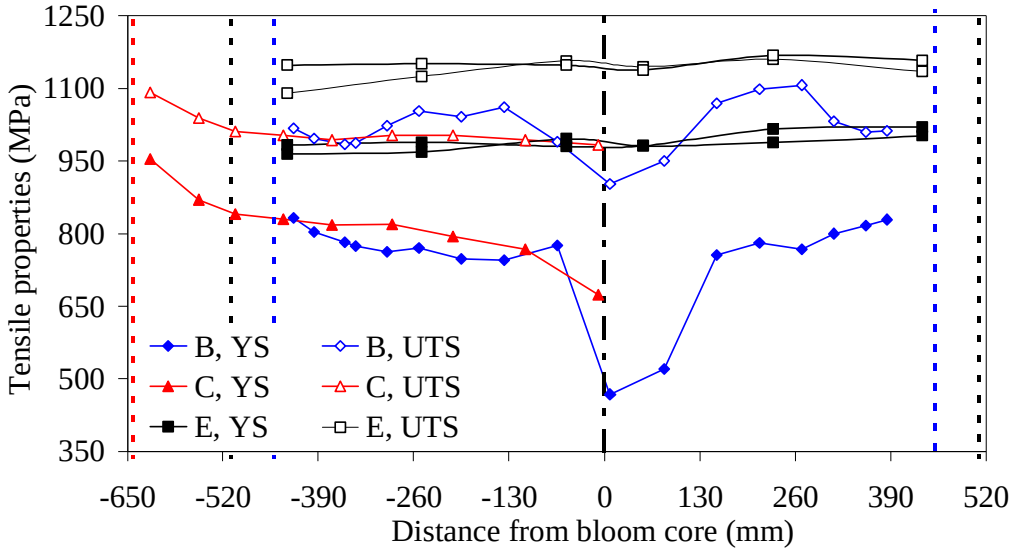

Fig. 2 – 1.2738 steel (B and C blooms) and E steel tensile strength (UTS) and yield stress (YS). Shaded lines represent the blooms core and surfaces.

The original microstructure of the examined part of D bloom is temper-modified bainite, with PAG boundaries evidenced by (supposed) carbide precipitates (Figs. 3a,b) and hardness, YS and UTS of 380 HV_{100}, 850 MPa and 1150 MPa, respectively. The laboratory re-heat-treated (RHT) samples consist mainly of tempered martensite, with some temper-modified bainite, scarcely evident PAG boundaries (Fig 3c) and hardness of 420 HV_{100}. No modifications due to aging

could be detected in the bloom material by optical microscopy, whereas the RHT material after aging generally exhibit a coarser carbide distribution and more evident PAG boundaries (Fig. 3d) than before aging.
At the examined temperatures, the age hardening of D steel generally is complete after ~1.5 h and the hardness is almost constant for aging durations up to 8 h; a slight overaging occurred only in the RHT steel at 550 °C (Fig. 4).
Aging at increasing temperatures yields larger hardness, YS and UTS values, but decreasing uniform elongation (El_u) and fracture elongation (El_t). Aged as-received and aged RHT samples have different El_u, YS and UTS for the same aging temperature, but these differences decrease at increasing aging temperature (Fig. 4 and 5). On the contrary, the El_t difference increases; in particular, aged as-received tensile samples fail without appreciable necking.
The amount of carbides detected by SEM [7] generally decreases by increasing the aging duration and temperature (for both as-received and RHT material). It is thought that carbides formed during prior heat treatments and unstable at the aging temperature are dissolved, while undetected finer carbides, possibly with different compositions, are re-precipitated, thus causing the hardening effects.
The second phases electrochemically extracted from the sample RHT and aged at 550 °C for 7 h showed XRD diffraction peaks ascribable to η-MoC, and possibly to V_7C_8. The EDS analysis of the same second phases compacted powder confirmed the occurrence of Mo and of lower amounts of V, Fe, Cr, Si. Hence, it is thought that η-MoC and possibly V_7C_8 are among the abovementioned carbides responsible for the age hardening of the D steel.

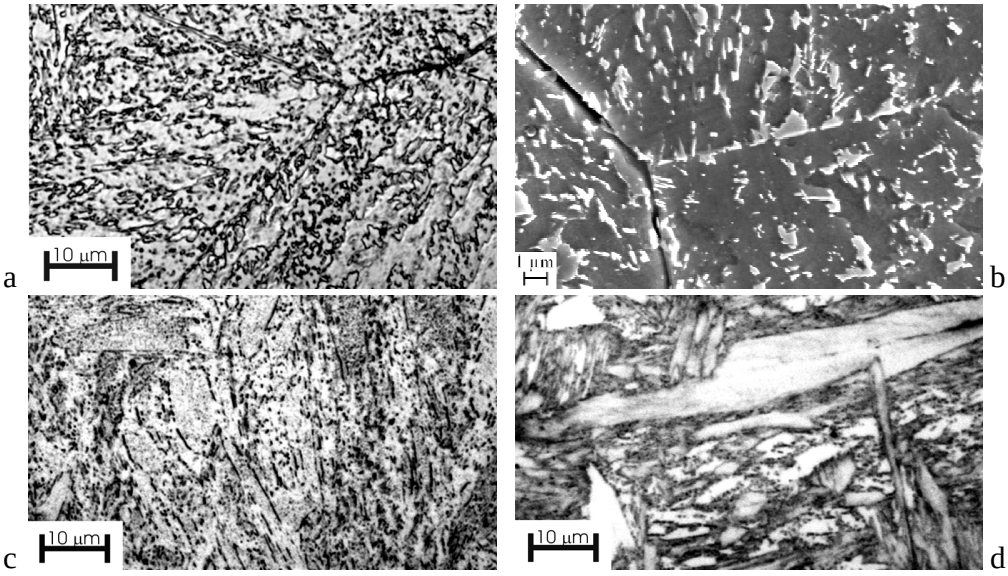

Fig. 3 – D steel. Microstructure of the original bloom (a,b), of Re-Heat-Treated (RHT) material (c) and of material RHT and aged at 550 °C for 5.5 h (d).

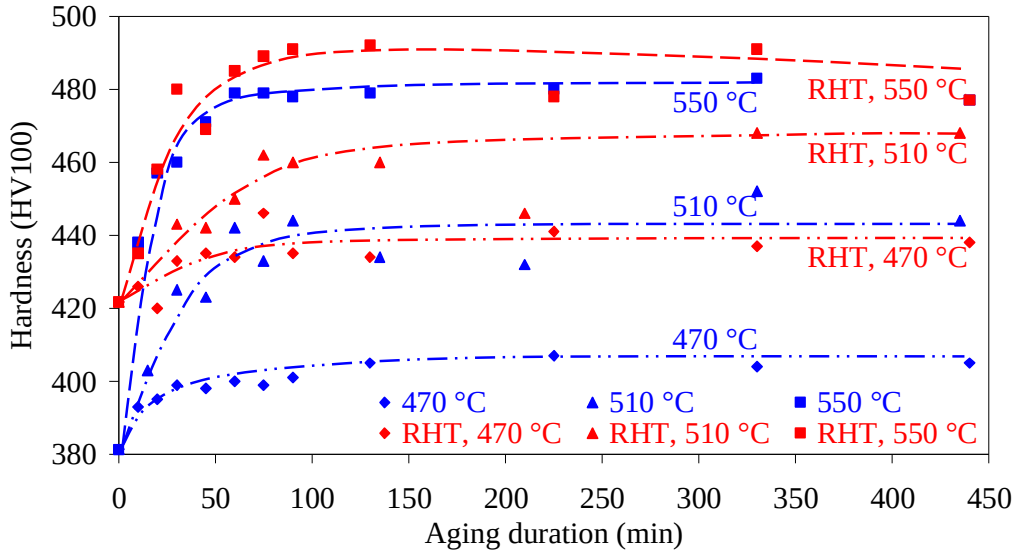

Fig. 4 – D Steel. Age-hardening of as received and re-heat-treated material.

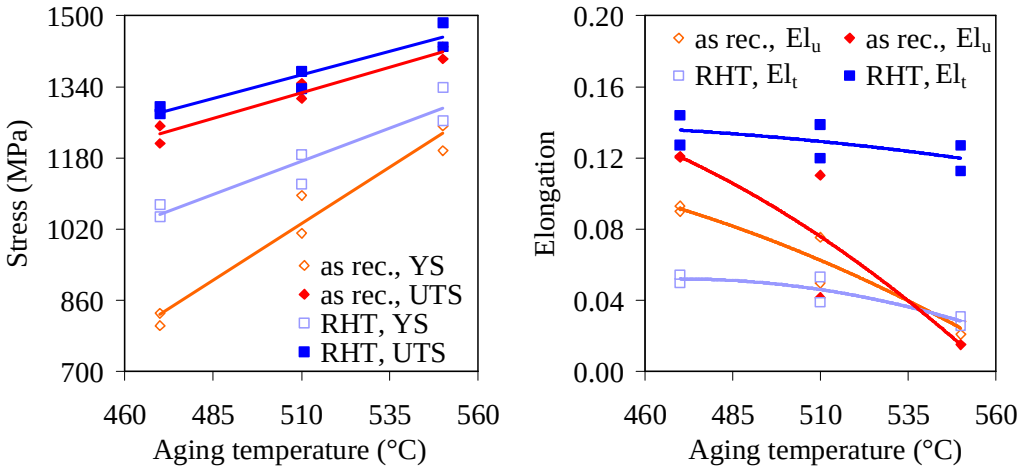

Fig. 5 – D Steel. Tensile properties in different conditions. Aging duration: 2.5 h.

4. Toughness and Fractography

The C bloom fracture toughness ranges from ~35 MPa√m at surface to ~45 MPa√m at core; the E bloom fracture toughness is similar at mid-depth and at core, but somewhat larger at surface (~55 MPa√m) (Fig. 6). These bloom values are much lower than the K_{Ic} of RHT (quenched and tempered) 1.2738 steel samples, even if the latter show a large scatter (86, 68, 103, 62 MPa√m). D bloom shows the largest K_{Ic}, i.e. 70 MPa√m (mean of 2 tests), but this decreases to 44 MPa√m (mean of 4 tests) after aging the bloom material at 525 °C for 3,5 h.
The lower toughness of the E bloom mid-depth and core regions, in respect to the surface region, is also evidenced by the much lower tensile reduction of area (Fig.

6), and by the lack of detectable necking in core tensile samples.
Plane-strain fracture surfaces of 1.2738 steel samples (obtained from C bloom) generally exhibit at the bloom surface mixed intergranular rupture (along supposed PAG facets) and cleavage; mainly cleavage at mid-depth; and cleavage mixed with an increasing fraction of ductile areas going from mid-depth to core, which may cause the moderate K_{Ic} increase toward the core. Tensile fracture surfaces of 1.2738 steel samples are always ductile.
The D steel plane-strain fracture surfaces (in the bloom condition) show mixed cleavage and microscopically ductile intergranular ruptures; the latter are prevalent in tensile fracture surfaces of as-received and aged samples, even if RHT and aged tensile samples show completely ductile fracture surfaces.
The E steel plane-strain fracture surfaces exhibit mainly cleavage, with some brittle intergranular zones, irrespective of the bloom depth; a similar morphology also occurs on the fracture surfaces of core tensile samples, whereas some ductile areas appear in mid-depth tensile samples and become prevalent in surface ones.
The occurrence of intergranular fracture may be related to elemental segregations at PAG boundaries [10], due to the long bloom heat treatment durations.
The plane-strain fracture surfaces of RHT 1.2738 steel samples, consisting of tempered martensite, similarly show mixed intergranular fracture and quasi-cleavage, but they also show a mode-II ductile tearing region at the pre-crack tip, which is absent in all other bloom materials; the width of this region is directly correlated with the K_{Ic} value, and this is probably the cause of the large K_{Ic} data scatter.

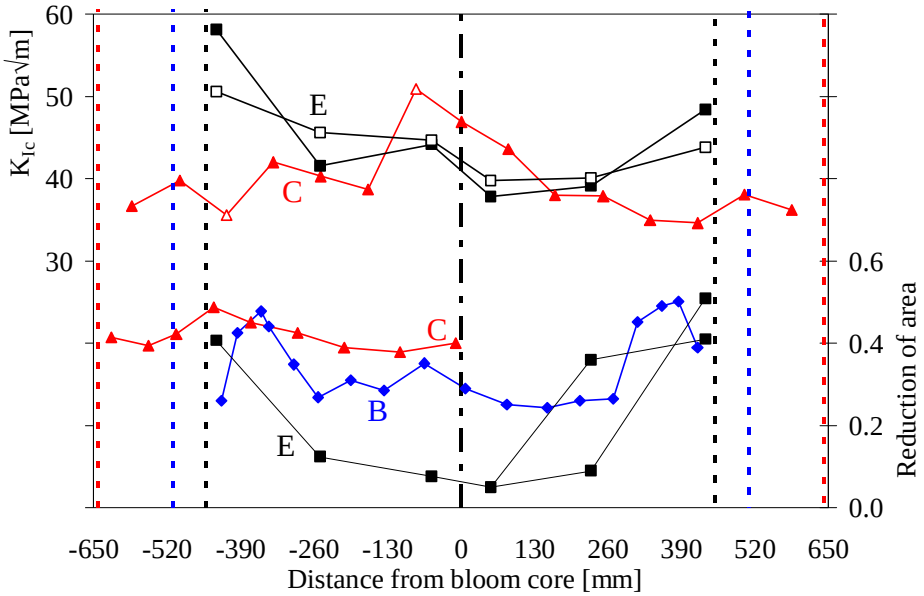

Fig. 6 – 1.2738 steel (B and C blooms) and E steel. K_{Ic} (empty symbols if $P_{max}/P_q > 1.1$) and reduction of area. Shaded lines represent the blooms core and surfaces.

5. Fatigue

E steel showed a rotating bending fatigue stress limit (50% survival after $4.2 \cdot 10^6$ cycles) of 630 MPa at surface and 565 MPa at core, whereas the corresponding values for the 1.2738 steel are 560 and 495 MPa for C bloom positions close to the surface and to the core, respectively. C bloom samples obtained from the same positions and re-heat-treated yield a about 25% larger fatigue limit, but, contrary to all other tests on RHT 1.2738 steel, maintain the difference among the original bloom position (700 and 610 MPa).
The FCG behavior of 1.2738 steel from C bloom and E steel are overall similar, except that steel E shows a slightly steeper Paris slope (Fig. 7).
These results are compared with those of SENB samples fabricated with 1.2738 steel subjected to different re-heat-treatments. The trend of tempered martensite is similar to that of the bloom microstructures (although the former breaks at a higher ΔK due to the higher K_{Ic}). Pearlite exhibits a similar slope in the linear range, but slower FCG, than the bloom core material which also contains some bainite. Finally, the bainitic sample, which also contains some martensite, shows a Paris slope ~3 times larger than all other ones and much faster FCG at high ΔKs.

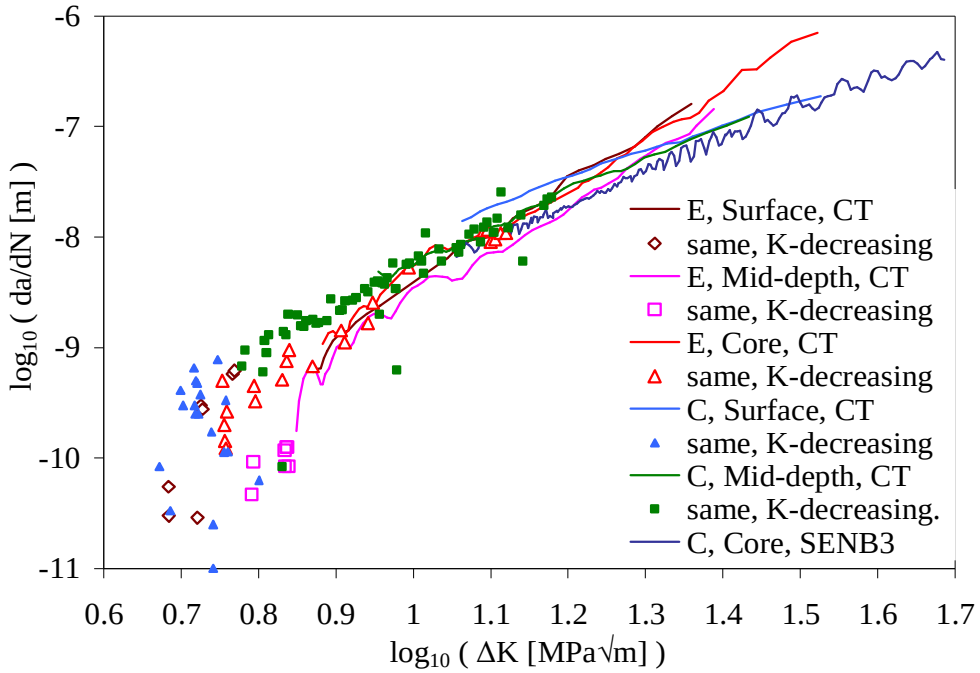

Fig. 7 – 1.2738 steel coming from C bloom and E steel. Paris (FCG) plot.

6. Discussion and Conclusions

The 1.2738 steel blooms generally show a large microstructure and strength

gradient from surface to core, and blooms obtained from different steelmaking practices may show large differences in the PAG size and in the presence of microstructural segregation. Moreover, the fracture toughness of the examined 1.2738 steel bloom is exceptionally low (about 40 MPa√m) for a quenched and tempered steel, considering the achieved UTS (985 – 1090 MPa).

The E steel bloom exhibits somewhat higher strength and remarkably more homogeneous microstructures and strength properties; however, in most of the bloom sections the fracture toughness is not much larger than that achieved by the1.2738 steel, and still much lower than the K_{Ic} of individually quenched and tempered 1.2738 steel samples. Moreover, E bloom shows a transition toward a more brittle fracture mode at core, whereas no such transition occurs in the 1.2738 steel case.

The as-received D steel exhibits the largest fracture toughness (70 MPa√m) among the examined bloom materials, together with acceptable strength and hardness. It is uncertain whether these properties are homogeneous, as expected from previous quench calculations [5,7], since no core material was examined.

The substantially asymptotic trend of the age hardening D steel hardness at the examined aging temperatures, for durations up to 8 h, may allow to obtain homogeneous results also in the aging of molds with large cross-section, for which the actual aging duration is differentiated from surface to core. Nevertheless, the aging treatment generally causes a relevant toughness reduction; thus the aging treatment may not always be advantageous in respect to the bloom metallurgical condition.

The largest mold stresses may be located away from the mold figure, in zones where large curvature radii are usually employed; thus, the steel's unnotched fatigue behavior is relevant for the nucleation and the initial propagation of subcritical defects in these zones. Thereafter, the defect propagation throughout the mold is determined first by the steel FCG behavior, and then by its K_{Ic}.

Both the unnotched fatigue strength and the fracture toughness are usually not mentioned in the plastic mold steel specifications, and thus designers may implicitly assume that these properties are similar to those encountered in low-alloy quenched and tempered carbon steels having the same tensile strength. On the contrary, present results show that in the metallurgical conditions encountered in large plastic mold steel blooms these properties may be lower, particularly for fracture toughness, in respect to those expected in smaller heat treated components, only the FCG behavior being substantially similar. Therefore, the verification of the mold designs against the brittle fracture risk, by using the fracture mechanics approach and taking into account the actual metallurgical conditions, should be recommended.

Acknowledgements

Italian Ministry for University and Research, for financial support by grants PRIN 2003091205 and 2005090102. H.C.M. Stampi, Moncalieri (TO), Italy, and

Lucchini Sidermeccanica, Lovere (BG), Italy, for steel procurement. M. Chiarbonello, for experimental work performed during his Ph.D. studies.

References

[1] ISO 4957:1999, Tool steels.
[2] D. Firrao, P. Matteis, M. Vassallo, 11th Int. Conf. Fracture, Torino, 2005
[3] M. Chiarbonello et al., proc. 16th Eur. Conf. Fracture, Alexandroupolis, 2006
[4] D. Firrao et al., Mater. Sc. Eng. A, 468-470 (2007), 193-200
[5] D. Firrao et al., proc. EPD symp., TMS Annual Meet., Orlando, 2007, 69-78
[6] D. Firrao et al., proc. 17th Eur. Conf. Fracture, Brno, 2008, 2357-2363
[7] D. Firrao et al., La Metallurgia Italiana, in press
[8] ASTM E399-05. Standard test method for plane-strain fracture toughness of metallic materials.
[9] ASTM E647-05, Standard test method for measurement of fatigue crack growth rates.
[10] C.L. Briant, S.K. Banerji, Int. Met. Reviews, No. 4, p 164-199, 1978.